Received: 00 Month 0000 | Revised: 00 Month 0000 | Accepted: 00 Month 0000

DOI: xxx/xxxx

ARTICLE TYPE

Laser Imaging Polarimetry of Nacre

Joshua A. Jones | Rebecca A. Metzler | Anthony J. D'Addario | Carrie Burgess | Brian Regan | Samantha Spano | Ben A. Cvarch | Enrique J. Galvez*,

[1]Department of Physics and Astronomy, Colgate University, HamiltonNew York 13346, U.S.A.

Correspondence
*Enrique J. Galvez. Email: egalvez@colgate.edu

Nacre is a complex biomaterial made of aragonite-tablet bricks and organic mortar that is considerably resilient against breakage. Nacre has been studied with a wide range of laboratory techniques, leading to understanding key fundamentals, and informing the creation of bio-inspired materials. In this article we present an optical polarimetric technique to investigate nacre, taking advantage of the translucence and birefringence of its micro-components. We focus our study on three classes of mollusks that have nacreous shells: bivalve (*Pinctada fucata*), gastropod (*Haliotis asisina* and *Haliotis rufescens*) and cephalopod (*Nautilus pompilius*). We sent polarized light from a laser through thin samples of nacre and did imaging polarimetry of the transmitted light. We observed clear distinctions between the structures of bivalve and gastropod, due to the spatial variation of their birefringence. The patterns for cephalopod were more similar to bivalve than gastropod. Bleaching of the samples disrupted the transmitted light. Subsequent refilling of the bivalve and gastropod nacre samples with oil produced optical patterns similar to those of unbleached samples. In cephalopod samples we found that bleaching produced irreversible changes in the optical pattern.

KEYWORDS:
Polarimetry, Imaging, Nacre, Shell

1 | INTRODUCTION

Nacre is a fascinating self-assembled structure in the natural world. It is a structure that was specialized by evolution to give shelled mollusks protection against predators and other causes threatening their survival. It is a remarkable structure that combines rigidity with toughness against breakage [1]. Many mollusk-shell organisms use inorganic materials such as calcium carbonate ($CaCO_3$) to build a nacreous structure in their shell. There are four classes of shelled organisms that have nacre: bivalves, gastropods, cephalopods and monoplacophorans. Bivalves, featuring two separate shells joined by a hinge, have a large contingent of species with nacre, such as clams and pearl oysters. Gastropods are single-shelled mollusks, with a small fraction of species having nacreous layers in their shells. They include popular examples, such as abalone and the great green turban. Cephalopods encompass a broader range of species, such as squids and octopuses, which do not have any nacre. One exception is *Nautilus pompilius*, a fascinating cephalopod species featuring a spiral-shaped chambered shell. It is the only species of its class that has an external shell. Monoplacophorans constitute a class of species that are mostly extinct, but some species with nacreous shells live in the deep ocean [2]. In this study we concentrate on shelled species from 3 of the 4 classes: *Pinctada fucata* for bivalves, *Haliotis asinina* and *Haliotis rufescens* for gastropods and *Nautilus pompilius* for cephalopods. Photos of the corresponding shells are shown in Fig. 1 .

Nacre is composed of ordered aragonite crystals and organic molecules. Aragonite belongs to the orthorhombic class of

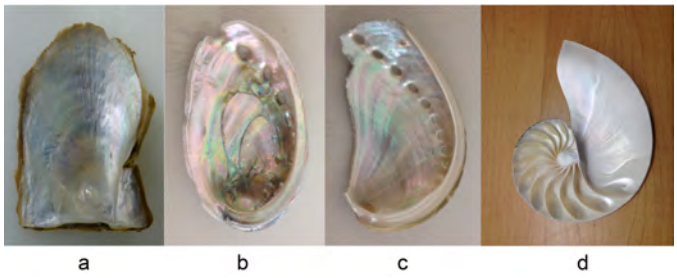

FIGURE 1 Images of the nacre side of the shells of *Pinctada fucata* (a), *Haliotis rufescens* (b), *Haliotis asinina* (c) and *Nautilus pompilius* (d).

biaxial crystals with distinct indices of refraction in the three mutually orthogonal optic axes a, b and c. The indices of refraction along these axes are: $n_a = 1.530$, $n_b = 1.681$ and $n_c = 1.685$ [3]. The microscopic design of nacre is a "brick and mortar" scheme consisting of a regular arrangement of aragonite tablets 5-10 μm in extension and 0.3-0.5 μm in thickness. Planar and cross-sectional views of the aragonite tablets in *Pinctada fucata* taken with an electron microscope are shown in Fig. 2 . The aragonite tablets are separated by 30-nm thick organic mortar made of long organic molecular chains [4, 5]. In most shells nacre forms only an inner fraction of the width of the shell. The outer fraction of the shell is composed of calcite crystals arranged in a semi-ordered way, constituting what is known as the the "prismatic" layer of the shell. In some species, such as the great green turban, nacre forms the entire width of the shell. Mollusk organisms build nacre by facilitating two basic self-assembled microscopic designs: sheet structure, deposited layer after layer; or columnar, where island columns of aragonite tablets first grow vertically to then proceed to grow transversely until the layers are all filled. In addition to the brick and mortar components, recent studies have found evidence of organic material located within each individual aragonite brick [6]. though the exact location of the organic material within the aragonite crystals is unknown. The formation mechanism is a complex self-assembly process in which organic elongated proteins such as chitin facilitate the conversion of amorphous calcium carbonate into aligned aragonite tablets [7].

The two designs have separate lineages dating back to their evolutionary separation in the Cambrian period (ca. 550 million years) [8]. In *Pinctada fucata* and other bivalve shells the bulk of the nacreous aragonite crystals are organized such that their optic c-axes are perpendicular to the aragonite tablets forming the shell surface, with their optic a- and b-axes aligned within a layer, but with smooth variations from layer to layer [9]. In gastropods the c-axis is also perpendicular to the tablets but the a- and b-axes are aligned only within a column, and differing from column to column [10, 11]. *Nautilus pompilius* is the only cephalopod known to have nacre [12], and its structure is believed to be columnar, similar to gastropod [13].

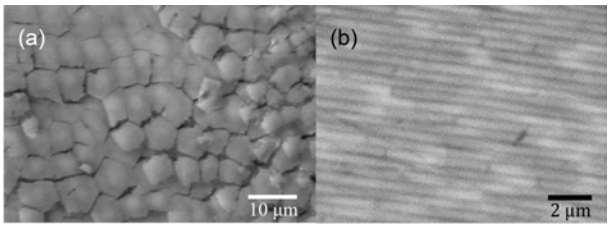

FIGURE 2 Electron microscope images of aragonite tablets in layered nacre (*Pinctada fucata*): (a) planar view and (b) cross section.

Nacre exhibits a colorful iridescence that is caused by diffraction and interference of light off the aragonite tablets and nacre's multilayered structure [14, 15]. Although these optical effects are byproducts of a material that evolved for its mechanical properties, they can be used to study its structure. The birefringent nature of calcite and aragonite crystals stacked together in these shells makes them amenable to their investigation using polarized light [16]. Here we present the use of a coherent polarimetric imaging technique to explore the alignment of optic axes of the tablets composing the shells [17]. This is similar to previous techniques that investigate materials via polarization-sensitive imaging [18, 19]. We complement our results with images from SEM and optical microscope. We use the results of polarimetric imaging to compare the structure of shells of different species.

2 | RESULTS

We studied the structure of nacre by sending polarized laser light through thin shell samples. Light was focused onto the sample illuminating a transverse area of a fraction of a millimeter in diameter. The polarization of the transmitted light was subsequently imaged with a digital camera.

The results presented here are representative of a study that involved multiple shells and multiple samples per shell. We explored all points of each sample.

2.1 | Bivalve Shell: *Pinctada fucata*

Figure 3 shows an example of the polarization patterns that were produced for each of the six input polarization states. The format of the images throughout the article is as follows. The false color of the images encode the orientation of the polarization ellipse (e.g., red = horizontal, green = diagonal, teal = vertical and blue = antidiagonal). The color saturation

encoded the intensity. We also show ellipses drawn at regular intervals representing the state of polarization the light at those points. We established a minimum intensity level for showing the ellipses. Otherwise they would appear in random shapes and orientations, which can be distracting.

The figure was produced with a shell sample of *Pinctada fucata*. Samples had thickness that ranged between 150 μm and 500 μm. We can see that the polarization pattern is very uniform across the beam profile, implying that the *a* and *b* crystalline axes of the aragonite tablets were uniform in the transverse plane. This has been found in previous studies using other methods [10]. This uniformity in the polarization is remarkable considering that the light had to pass through a large number of aragonite tablets: between 10,000 and 100,000 depending on the beam and sample dimensions.

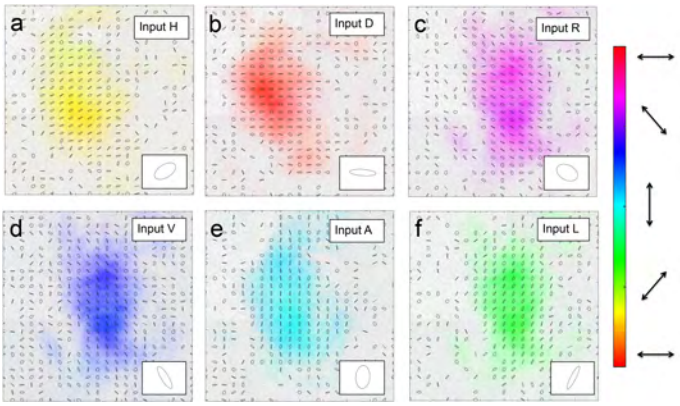

FIGURE 3 Polarimetry results for *Pinctada fucata* with each of the six encoded input states: (a) linear vertical (V), (b) linear antidiagonal (A), (c) linear horizontal (H), (d) linear diagonal (D), (e) right circular (R), and (f) left circular (L). Ellipses denote the polarization of light at the corresponding image point, color indicates orientation of polarization ellipse, and saturation corresponds to the intensity of the light.

As described in a later section, we obtained the 4×4 Mueller matrix of the illuminated portion of the shell samples. The relations between the values of the Mueller matrix elements m_{ij} specify particular optical transformations. A few examples are shown in the list below:

- Unitary optical element (i.e. without absorption): $m_{11} = 1$ and $m_{12} = m_{13} = m_{14} = m_{21} = m_{31} = m_{41} = 0$.
- Retarder (a general birefringent optical element): $m_{32} = m_{23}$, $m_{42} = -m_{24}$ and $m_{43} = m_{34}$, with $m_{22} \neq m_{33} \neq m_{44}$.
- Rotator: $m_{22} = m_{33} \neq 0$, $m_{23} = -m_{32}$, $m_{44} = 1$ and $m_{24} = m_{34} = m_{42} = m_{43} = 0$.

A monolithic birefringent material would likely behave as retarder due to the difference in the index of refraction along orthogonal axes. The regular structure of bivalve shells, with all their optic axes aligned within a layer is likely to approach that of a monolithic retarder. However, the layered structure also allows a progressive rotation of the *a* and *b* axes from layer to layer, analogous to cholesteric liquid crystals, making it also behave as a rotator. In Fig. 4 we show the computed Mueller matrix corresponding to the imaged data of the *Pinctada fucata* shell sample that yielded the results of Fig. 3 .

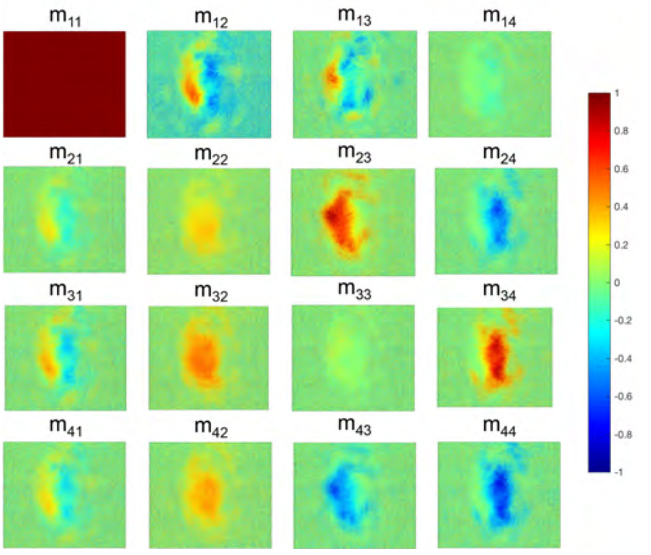

FIGURE 4 Mueller matrix corresponding to the data of Fig. 3 . The size of the image is 960×1280 pixels.

An evaluation of the matrix $\boldsymbol{M}$ of an average of values of each point in a central region of the images measuring 200×200 pixels gives

$$\begin{pmatrix} 1.00 & -0.10 \pm 0.29 & -0.15 \pm 0.15 & -0.04 \pm 0.11 \\ -0.03 \pm 0.16 & 0.31 \pm 0.12 & 0.45 \pm 0.23 & -0.37 \pm 0.17 \\ -0.06 \pm 0.21 & 0.50 \pm 0.14 & 0.02 \pm 0.10 & 0.55 \pm 0.23 \\ -0.07 \pm 0.18 & 0.41 \pm 0.12 & -0.32 \pm 0.17 & -0.50 \pm 0.20 \end{pmatrix}. \quad (1)$$

The uncertainties are the standard deviation of the measurements. The matrix reveals some of the characteristics of the retarder, such as combination of matrix elements that should give zero: $m_{23} + m_{32} = -0.05 \pm 0.23$, $m_{42} - m_{24} = 0.04 \pm 0.20$, and $m_{34} + m_{43} = 0.22 \pm 0.35$. Three diagonal elements besides the first one add to 1: $m_{22} + m_{33} - m_{44} = 0.82 \pm 0.25$. Finally, m_{1i} and m_{i1} ($i = 2, 3, 4$) are consistent with zero, as expected. Even smaller subsets are consistent with these values. A monolithic retarder with a retardance of 134 ± 7 degrees oriented 18 ± 3 degrees would have a matrix similar to the one shown in Eq. 1. The inserts to the panes of Fig. 3 are states computed with

these retardance values. As can be appreciated from comparing the calculated ellipses with the measured ones, the values extracted from the Mueller matrix are consistent with the data. We have done similar experiments with a monolithic sample of calcite and found consistent results. Our findings reported in a previous conference proceeding also show the rotator behavior in nacre samples [17].

2.2 | Gastropod Shell: *Haliotis asinina and Haliotis rufescens*

The columnar structure of nacre in gastropods is optically quite distinct from the layered bivalve. The nonalignment of the *a* and *b* axes from column to column, separated by as low as 5-10 μm, transforms the polarization of the incoming light in a way that varies within the beam width. We have not modeled this process, but we imagine that optically it behaves like a material with a honeycomb type structure where each cell, a columnar stack of tablets, is a birefringent column, with retardance varying from column to column. This honeycomb picture is only idealized because in reality the stacks are not necessarily straight columns. Our optical beams were focused in such a way that the light had a planar wavefront as it passed through the sample. Due to its transverse extension, the light beam may go through 100-500 columnar domains.

The light beam transmitted through the gastropod-shell sample showed a broad speckle pattern. Figure 5 shows representative patterns of the polarization of the light transmitted through *Haliotis asinina* (a,b) and *Haliotis rufescens* (c,d). The patterns are quite irregular compared to the uniform patterns produced by the bivalve shell (Fig. 3). Each pattern contains illuminated regions of predominantly smoothly-changing polarization. The pattern has similar spatial extent for distinct input states of polarization. The domains vary in size as we vary the input polarization, but they are quite broad. These results imply that the light undergoes a complex refractive process as it travels through the sample.

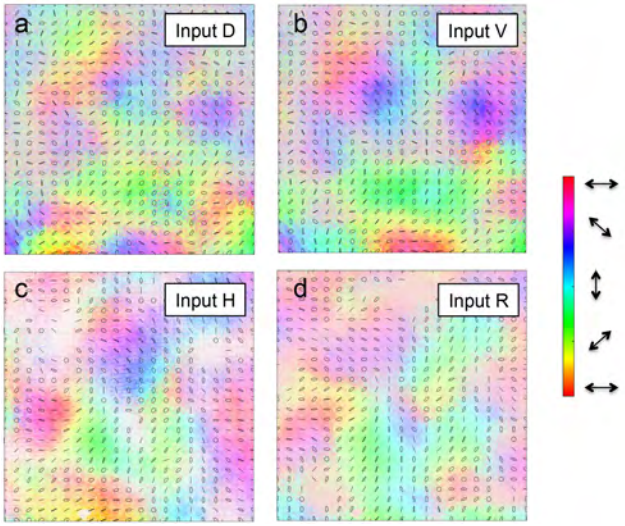

FIGURE 5 Polarimetry data of light passing through shells *Haliotis asinina* in (a,b) and *Haliotis rufescens* in (c,d) for different input polarization states, respectively. Color encodes orientation and saturation encodes intensity.

2.3 | Cephalopod Shell: *Nautilus pompilius*

Figure 6 shows the results for two distinct samples of *Nautilus pompilius*, (a,b) and (c,d), taken from the same shell. The polarization pattern of the transmitted light is puzzlingly similar to that of bivalve nacre. A further puzzling result is that the samples barely showed any birefringence: in all cases the output polarization was close to the input polarization. The Mueller matrix of the shell showed a more complex birefringence than what would be expected from the figure, perhaps implying that a fortuitous optical cancellation rather than a non-birefringent transformation is responsible for the observations. These measurements were repeated with three separate samples, finding consistent results in all of them. The uniformity of the patterns suggests that the columnar regions all have their optic axes aligned. The apparent lack of birefringence could be explained if the two axes with similar index of refraction (*b* and *c*) were contained in the plane of the aragonite tablets. However, this contradicts previous findings [13].

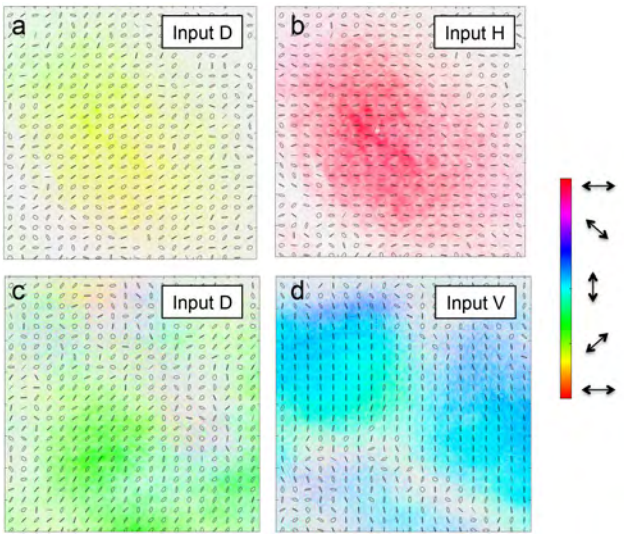

FIGURE 6 Polarimetry data of light passing through *Nautilus pompilius* shell: in two separate samples (a,b) and (c,d) for different input polarization states, respectively. Color encodes orientation and saturation encodes intensity.

2.4 | Bleaching and Refilling

We investigated the optical role of the organic mortar in between the aragonite tablets by bleaching the samples. We took polarimetric images of each sample before and after bleaching. In Fig. 7 we show the results for bivalve in (a), gastropod in (b) and cephalopod in (c). The polarization of the bleached-sample images changes rapidly from point to point, consistent with significant light scattering. The polarization appears randomized, as expected from multiple scattering of polarized light. The polarization of bleached gastropod samples appeared much more randomized than those of bivalve and cephalopod samples, as can be seen in comparing images (a) and (c) with (b).

We further refilled the bleached samples to test if bleaching permanently affected the structure of the shell. We then redid the polarimetry imaging with the refilled samples. Here we saw a significant difference between either bivalve or gastropod and cephalopod. For all the bivalve and gastropod shells we investigated, the polarization pattern resulting from the refilled shell showed no significant difference from the ones observed before bleaching. Figures 7 (d) and (e) show the images of the refilled samples corresponding to those in panes (a) and (b), respectively. Conversely, the refilled samples of *Nautilus pompilius* did not return to their original state. If it were to return to the original pattern we would expect a pattern similar to Figure 7 (d). Instead, it looks more like those of Figure 7 (e).

These results leads us to conclude that the immersion oil plays the same optical role as the organic matter of optically blending the space in between tablets. For bivalves and gastropods nacre does not seem to rely on the organic mortar to support the tablet structure. Mineral bridges must support the tablet locations independently of the presence of organic matter [1, 13]. The results for cephalopod nacre show that bleaching causes irreversible changes in the pattern. This implies that organics in cephalopod play a vital role in holding aragonite tablets together, to the point that in the aragonite tablets lose their original relative position or orientation when bleached.

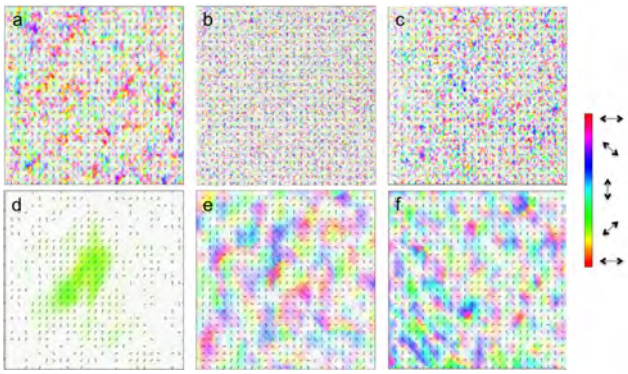

FIGURE 7 Polarimetry images for samples of *Pinctada fucata* in (a) and (d), *Haliotis asinina* in (b) and (e), and *Nautilus pompilius* in (c) and (f). The samples were bleached in (a)-(c), and refilled with oil in (d)-(f). Ellipses denote the polarization of light at the corresponding image point, color indicates orientation of polarization ellipse, and saturation corresponds to the intensity of the light.

3 | DISCUSSION AND CONCLUSIONS

In summary, we used optical polarimetry to study the structure of nacre in several shelled species. This was possible due to two optical properties of this self-assembled biomineral: transparency and birefringence. We found that *Pinctada fucata* behaved like a transversely uniform optical sample. This confirms the general understanding of the structure of bivalve shells: a full alignment of the crystallographic axes of aragonite tablets arranged in a layered fashion. Rotator properties observed in some samples implies that the transverse optic axes often rotate smoothly through the layers. The light going through the nacre of gastropod shells *Haliotis asinina* and *Haliotis rufescens* is consistent with a birefringence that varies transversely along the biomineral. This confirms the distinction between bivalve and gastropod: gastropods have a columnar structure of aragonite tablets with optic axes that vary from column to column, as opposed to the transversely uniform birefringence of bivalves. These transverse variations of gastropods may be more gradual than sharp, because the polarization of the light traversing the shell is not fully randomized but it retains a certain degree of order. We find that cephalopod *Nautilus pompilius* has an optical behavior similar to the bivalve shells, contrary to the expectation, given their columnar structure [13], with the additional oddity that apparently it does not affect significantly the polarization of the input light; findings that prompt further investigation. These results could be reconciled if the alignment of optical axes of the aragonite tablets is the same from column to column.

We found that bleaching the sample destroys the polarization order of the transmitted light. We attribute this depolarization to multiple scattering. Refilling the bleached sample with index-matching fluid made the nacre of bivalve and gastropod shells regain the optical properties they had prior to bleaching, implying that the removal of organic matter did not affect the relative position of the aragonite tablets. This is likely due to mineral bridges that are not affected by the bleaching action, which keep much of the nacre structure in place. Our results also show that cephalopod nacre gets visibly affected by bleaching, implying a distinct structural composition that relies on organic matter to hold nacre together.

In conclusion, optical polarimetric data confirm previous understanding of the composition of nacre and further adds

new clues on its structure that have not been obtained by other methods.

4 | METHODS

4.1 | Shell Sample Preparation

We prepared thin samples of shells purchased from a commercial vendor (cnpearls.com). Each shell was fractured to find flat samples that were about 1-cm in size. The samples were cleaned with ethanol and polished on the outer prismatic side until the nacre layers were reached. The total thickness of the samples varied between 0.3 and 0.5 mm. We did the polishing by hand on silicon papers lubricated with deionized water. This stage used papers with 600-1200 grit. A final polish was accomplished with a nylon pad and 50-nm alumina slurry. This eliminated scratches that would produce scattering. We verified this with an optical microscope. The inner nacre layer was either left intact or lightly polished to remove any scratches. A photo of a sample of *Pinctada fucata* is shown as an insert to Fig. 8 .

4.2 | Bleaching

The samples were bleached by submersing them in a sodium hypochlorite solution to remove the organic mortar located in between the aragonite tablets. The samples did not come apart, suggesting other links between tablets, such as mineral bridges, hold the tablets together [1]. It should be noted that the prismatic layer of *Pinctada fucata* shells placed in bleach dissolved into individual crystals while the aragonite tablets of nacre did not. After the bleaching, the sample exhibited a cloudy appearance [17], a sign of significant light scattering. A careful look at the sample of *Pinctada fucata* taken after bleaching with the scanning electron microscope, shown in Fig. 2 a, indeed showed gaps between the aragonite tablets. After the optical analysis of the bleached shell we refilled it with oil. This was done by immersion into type-A non-drying immersion oil, of refractive index 1.5114 [20], under vacuum to fill the gaps between the aragonite tablets.

4.3 | Optical technique

Our technique consisted of preparing a laser beam in a definite state of polarization, focusing it, and passing it through thin samples of nacre, as shown in Fig. 8 . We then imaged the polarization of the transmitted beam, which in the most general case varied across the beam. This method is similar to the one used in a previous study [16], but with important differences: in this work we used longer focal length for the focusing and recollimating lenses (L_3 and L_4) so that the wavefront remained close to that of a plane wave as the light passed through the samples. The polarization analysis of the two studies is also different.

The optical beam was generated by a linearly-polarized helium-neon laser (HeNe, of wavelength 633 nm). After passing the beam through a neutral density intensity filter (F) and steered by two mirrors (M_1 and M_2), the beam was sent through two lenses (L_1 and L_2) to expand it to a 1-mm spot size, as shown in Fig. 8 . It was subsequently sent through a polarizer oriented vertical (P_1) followed by a quarter-wave plate (Q_1) and a half-wave plate (H_1). These prepared the beam in one of six polarizations states: linear vertical (V), linear horizontal (H), linear antidiagonal (−45°; A), linear diagonal (+45°; D), right circular (R), or left circular (L).

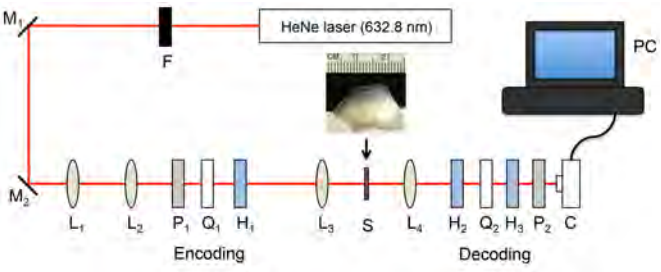

FIGURE 8 Schematic of the optical setup. A HeNe laser beam is steered by mirrors (M_1, M_2), expanded by lenses L_1 and L_2, focused by lens L_3 onto the sample (S; shown in photo insert), and imaged by lens L_4 into a digital camera (C). Polarization optics composed of polarizers (P), quarter-wave plates (Q), and half-wave plates (H) were used to encode and decode respectively the initial and final states of polarization of the light.

The polarized beam was focused with a lens (L_3, of 8.5-cm focal length) to a beam waist of 50-100 μm at the sample. A lens placed after the sample (L_4, of 8.5-cm focal length) imaged the light onto a digital camera (C). Before reaching the camera the beam traveled through a polarization-decoding stage consisting of two half-wave plates (H_2 and H_3), a quarter-wave plate (Q_2), and a polarizer (P_2). The decoding stage is a polarization filter. We took images with each of the filter states yielding intensity values I_H, I_V, I_A, I_D, I_R and I_L for each pixel. They were then used to obtain the Stokes parameters:

$$S_0 = I_H + I_V \quad (2)$$

$$S_1 = I_H - I_V \quad (3)$$

$$S_2 = I_D - I_A \quad (4)$$

$$S_3 = I_R - I_L, \quad (5)$$

from which we could obtain the polarization ellipse parameters. One parameter is the ellipticity of the polarization, defined

as

$$\epsilon = \pm\frac{b}{a} = \tan^{-1}\left(\frac{S_3}{\sqrt{S_1^2 + S_2^2 + S_3^2}}\right), \quad (6)$$

where b is the semi-minor axis and a is the semi-major axis of the polarization ellipse. The other parameter is the orientation of the polarization ellipse relative to the horizontal, given by

$$\theta = \frac{1}{2}\tan^{-1}\left(\frac{S_2}{S_1}\right). \quad (7)$$

We used a particular 3-waveplate system to decode the polarization because the two half-wave plates H_2 and H_3 specify respectively the ellipticity and orientation of the polarization ellipse [21]. This allowed greater flexibility in diagnosing the polarization pattern of the light even before obtaining the Stokes parameters [22]. For a given input polarization, the images taken with six filters were further processed to determine the polarization at each imaged point. We took data with the 6 input polarization states to obtain the Mueller matrix corresponding to the shell. The elements the Mueller matrix are defined in Table 1 [23, 24]. The Mueller matrix allowed us to obtain the polarization transformation applied by the shell, as discussed in the previous section.

TABLE 1 Matrix elements of the Mueller matrix expressed in terms of the measured intensities. The first and second subindices in the terms (e.g., I_{HH}) represent the polarization the incident and detected state, respectively.

Element	Definition
m_{11}	$0.5(I_{HH} + I_{HV} + I_{VH} + I_{VV})$
m_{12}	$0.5(I_{HH} + I_{HV} - I_{VH} - I_{VV})$
m_{13}	$0.5(I_{DH} + I_{DV} - I_{AH} - I_{AV})$
m_{14}	$0.5(I_{LH} + I_{LV} - I_{RH} - I_{RV})$
m_{21}	$0.5(I_{HH} + I_{VH} - I_{HV} - I_{VV})$
m_{22}	$0.5(I_{HH} + I_{VV} - I_{VH} - I_{HV})$
m_{23}	$0.5(I_{DH} + I_{AV} - I_{AH} - I_{DV})$
m_{24}	$0.5(I_{LH} + I_{RV} - I_{RH} - I_{LV})$
m_{31}	$0.5(I_{HD} + I_{VD} - I_{HA} - I_{VA})$
m_{32}	$0.5(I_{HD} + I_{VA} - I_{HA} - I_{VD})$
m_{33}	$0.5(I_{AA} + I_{DD} - I_{DA} - I_{AD})$
m_{34}	$0.5(I_{LD} + I_{RA} - I_{LA} + I_{RD})$
m_{41}	$0.5(I_{HL} + I_{VL} - I_{HR} - I_{VR})$
m_{42}	$0.5(I_{HL} + I_{VR} - I_{VL} - I_{HR})$
m_{43}	$0.5(I_{AR} + I_{DL} - I_{AL} - I_{DR})$
m_{44}	$0.5(I_{LL} + I_{RR} - I_{RL} - I_{LR})$

ACKNOWLEDGMENTS

We thank C. Jahncke for insightful discussions and B. Holmes for help. This work was funded by the Picker Interdisciplinary Institute of Colgate University.

Author contributions

E.G. and R.M. conceived the experiments; C.B., A.D., R.M. and S.S. prepared the samples; C.B., B.C., A.D., E.G., J.J., B.R. and S.S. took data and C.B., A.D., E.G., J.J., B.R. and S.S. analyzed the data.

Financial disclosure

None reported.

Conflict of interest

The authors declare no potential conflict of interests.

References

[1] Sun, J. & Bhushan, B. Hierarchical structure and mechanical properties of nacre: a review. RSC Adv. **2**, 7617–7632 (2012).

[2] Checa, A. G., Ramírez-Rico, J., González-Segura, A. & Sánchez-Navas, A. Nacre and false nacre (foliated aragonite) in extant monoplacophorans (=tryblidiida: Mollusca). *Naturwissenschaften* **96**, 111–122 (2009).

[3] *Optical waves in crystals* (John Wiley & Sons Inc., Hoboken, 2003).

[4] Gilbert, P. U. P. A. *et al.* Gradual ordering in red abalone nacre. *J. Am. Chem. Soc.* **130**, 17519–17527 (2008).

[5] Levi-Kalisman, Y., Falini, G., Addadi, L. & Weiner, S. Structure of the nacreous organic matrix of a bivalve mollusk shell examined in the hydrated state using cryo-tem. *J. Struct. Bio.* **135**, 8–17 (2001).

[6] Pokroy, B., Quintana, J. P., Caspi, E. N., Berner, A. & Zolotoyabko, E. Anisotropic lattice distortions in biogenic aragonite. *Nat. Mater.* **3**, 900–902 (2004).

[7] Addadi, L., Joester, D., Nudelman, F. & Weiner, S. Mollusk shell formation: a source of new concepts for understanding biomineralization processes. *Chem. Eur. J.* **12**, 980–987 (2006).

[8] Jackson, D. J. *et al.* Parallel evolution of nacre building gene sets in molluscs. *Mol. Bio. Evol.* **27**, 591 (2010).

[9] Checa, A. G. & Rodriguez-Navarro, A. B. Self-organisation of nacre in the shells of pterioida (bivalvia: Mollusca). *Biomaterials* **26**, 1071–1079 (2005).

[10] Cartwright, J. & Checa, A. The dynamics of nacre self-assembly. *J. R. Soc. Interface* **4**, 491–504 (2007).

[11] Metzler, R. A. *et al.* Architecture of columnar nacre, and implications for its formation mechanism. *Phys. Rev. Lett.* **98**, 268102 (2007).

[12] Velázquez-Castillo, R., Reyes-Gasga, J., García-Gutierrez, D. & Jose-Yacaman, M. Nanoscale characterization of nautilus shell structure: An example of natural self-assembly. *J. Mater. Res.* **21**, 1484–1489 (2006).

[13] Checa, A., Cartwright, J. H. & Willinger, M.-G. Mineral bridges in nacre. *J. Struct. Bio.* **176**, 330–339 (2011).

[14] Tan, T. L., Wong, D. & Lee, P. Iridescence of a shell of mollusk haliotis glabra. *Opt. Express* **12**, 4847–4854 (2004).

[15] Liu, Y., Shigley, J. E. & Hurwit, K. N. Iridescence color of a shell of the mollusk pinctada margaritifera caused by diffraction. *Opt. Express* **4**, 177–182 (1999).

[16] Metzler, R. A., Jones, J. A., D'Addario, A. J. & Galvez, E. J. Polarimetry of pinctada fucata nacre indicates myostracal layer interrupts nacre structure. *R. Soc. Open Sci.* **4**, 160893 (2017).

[17] Metzler, R. A., Burgess, C., Regan, B. & Spano, S. Polarimetry of nacre in iridescent shells. *Proc. SPIE* **9187**, 918704 (2014).

[18] Shribak, M. & Oldenbourg, R. Techniques for fast and sensitive measurements of two-dimensional birefringence distributions. *Appl. Opt.* **42**, 3009–3017 (2003).

[19] Mehta, S. B., Shribak, M. & Oldenbourg, R. Polarized light imaging of birefringence and diattenuation at high resolution and high sensitivity. *J. Opt.* **15**, 094007 (2013).

[20] http://www.cargille.com.

[21] Galvez, E. J., Khadka, S., Schubert, W. H. & Nomoto, S. Poincaré-beam patterns produced by non-separable superpositions of Laguerre-Gauss and polarization modes of light. *Appl. Opt.* **51**, 2925–2934 (2012).

[22] Jones, J. A., D'Addario, A. J., Rojec, B. L., Milione, G. & Galvez, E. J. The poincaré-sphere approach to polarization: Formalism and new labs with poincaré beams. *Am. J. Phys.* **84**, 822–835 (2016).

[23] Bickel, W. & Bailey, W. Stokes vectors, mueller matrices, and polarized scattered light. *Am. J. Phys.* **53**, 468–478 (1985).

[24] Hielscher, A. *et al.* Diffuse backscattering mueller matrices of highly scattering media. *Opt. Express* **1**, 441–453 (1997).